

# Experimental Cyclic Behavior of Precast Hybrid Beam-Column Connections with Welded Components

Sadik Can Girgin\*, Ibrahim Serkan Misir, and Serap Kahraman

(Received January 10, 2016, Accepted January 31, 2017, Published online May 22, 2017)

**Abstract:** Post-earthquake observations revealed that seismic performance of beam-column connections in precast concrete structures affect the overall response extensively. Seismic design of precast reinforced concrete structures requires improved beam-column connections to transfer reversed load effects between structural elements. In Turkey, hybrid beam-column connections with welded components have been applied extensively in precast concrete industry for decades. Beam bottom longitudinal rebars are welded to beam end plates while top longitudinal rebars are placed to designated gaps in joint panels before casting of topping concrete in this type of connections. The paper presents the major findings of an experimental test programme including one monolithic and five precast hybrid half scale specimens representing interior beam-column connections of a moment frame of high ductility level. The required welding area between beam bottom longitudinal rebars and beam-end plates were calculated based on welding coefficients considered as a test parameter. It is observed that the maximum strain developed in the beam bottom flexural reinforcement plays an important role in the overall behavior of the connections. Two additional specimens which include unbonded lengths on the longitudinal rebars to reduce that strain demands were also tested. Strength, stiffness and energy dissipation characteristics of test specimens were investigated with respect to test variables. Seismic performances of test specimens were evaluated by obtaining damage indices.

**Keywords:** beam-column connections, precast concrete, welding, unbonded length, damage index.

## 1. Introduction

One-story precast concrete structures constitute a significant part of industrial buildings in earthquake-prone regions in Turkey. Post-earthquake observations revealed that beam-column connections are widely influence the overall seismic response of precast concrete structures (Saatcioglu et al. 2001; Ozden and Meydanli 2003; Senel and Palanci 2013). It is still a challenging subject to develop precast concrete beam-column connections emulating the seismic performance of monolithic systems to maintain advantages of precast construction process for multi-story buildings.

In the literature, *joint* is defined as the intersection of beam and column elements while *connection* is the region where precast elements connected with a technique (welding, bolting etc.) during construction. Moment-resisting beam-column connections can be categorized mainly as *emulative (wet)* and *dry* connections (e.g. ACI 550.2R 2013). In addition, emulative and mechanical components can be assembled to constitute *hybrid beam-column connections* (Negro and Toniolo 2012) which are commonly used in Turkey.

In emulative connections, continuity of reinforcing bars is provided by a coupling connector or splicing throughout the designated gaps in precast beam and column elements at a precast construction facility. Precast beams are firstly supported on columns' cover concrete and then the topping concrete is poured on site to fill the gaps in the column and the top of the beam (Park and Bull 1986; Chen et al. 2012). Im et al. (2013) tested five interior precast beam-column connections with U-shaped beam shells. Main test parameters were seating length of beam to joint, steel angle for cover concrete and installation of headed rebars. It was concluded that increase in effective depth of beam-column connection can be obtained by decreasing the seating length and the beam shell thickness.

Dry beam-column connections are achieved by connecting the precast elements with post-tensioning, welding or embedded rods. Chang et al. (2013) presented experimental results of two full-scale interior beam-column connections with embedded ductile rods within the joint region. Main test parameters were the use of high strength concrete, post-tensioning and high performance reinforcing steel. They were concluded that specimens sustained large drifts without any strength degradation. Experimental studies on post-tensioned connections showed that increase in mild reinforcement ratio results in improved ductility and energy dissipation capacities. However, in some cases premature buckling and rupture of mild reinforcement may occur before reaching the drift ratios that the connection can

---

Department of Civil Engineering, Dokuz Eylul University, 35160 Buca-Izmir, Turkey.

\*Corresponding Author; E-mail: sadik.girgin@deu.edu.tr

Copyright © The Author(s) 2017. This article is an open access publication

sustain (Cheok et al. 1993; Priestley et al. 1999; ACI T1.2 2003; Ertas et al. 2006). It is proposed that, unbonding of reinforcing bars over a length of precast beam and column elements in a sleeve can reduce the strain demands and prevent rupture which leads significant degradation in strength (Cheok et al. 1996; Pampanin et al. 2001; Belleri et al. 2012). However, *unbonded length* should be selected properly to ensure yielding of reinforcing bars without premature rupture (Cheok et al. 1993).

In the third category, hybrid (emulative-welded) connections are widely used in residential and industrial frame structures where negative moment continuity is made through cast-in-place connection while positive moment continuity is satisfied through welding. Figure 1 shows a fabrication process of a precast structure by applying hybrid connections with the stages from precast facility to site. First, beam longitudinal and transverse rebars are welded to beam end plates and the remaining rebars in beam elements are installed (Fig. 1a, b). At the meantime, precast columns with corbels of hybrid connections are prepared and a gap is deliberately left at the top of the joint before casting of concrete to fill with topping concrete (Fig. 1c). After transportation and installation of precast beam, column, and slab elements, continuity between these elements are provided by pouring topping concrete in each floor level (Fig. 1d).

Seismic behavior of precast connections is required to be proved by experimental or numerical studies in terms of equivalent strength and ductility reflecting the monolithic behavior as specified in seismic codes (TEC 2007; ACI 318 2011). There has been a great deal of research by means of

experimental and numerical studies on reinforced concrete beam-column joints (Ronagh and Baji 2014; Kim and Hyunhoon 2015; Kassem 2015; Rashidian et al. 2016; Lim et al. 2016). However, there are a limited number of experimental studies on the behavior of hybrid (emulative-welded) connections in the literature. Ertas et al. (2006) tested half-scaled one exterior beam-column connection where the first diagonal crack near the connection was reported at 2.2% drift ratio and the beam bottom rebars ruptured at the first cycle of 3.5% drift ratio. Yuksel et al. (2015) tested five half-scaled exterior hybrid connections including a slab which are subjected to monotonic and cyclic drifts applied at the beam tip. Monotonic and cyclic tests on first three specimens showed that strength degradation occurs due to rupture of welded longitudinal rebars and transverse rebars at the connection. Improved specimens showed an increased energy dissipation capacity while the observed in-cycle degradation was about 50% at a drift ratio of 3%. During the tests, increase in strain demands of beam welded rebars played an important role for overall behaviors of the connections.

Experimental studies on welded ASTM A615 type reinforcing bars (ASTM 1992) revealed that welding process causes heat-affected zone on reinforcements following an embrittlement on the material which is undesirable for a ductile seismic design (Rodriguez and Rodriguez 2006; Rodriguez and Torres-Matos 2013). This kind of rebars showed a decreased tensile strain capacity in the vicinity of the welded region. However, welding is still a common used technique in connecting the steel parts of structural elements

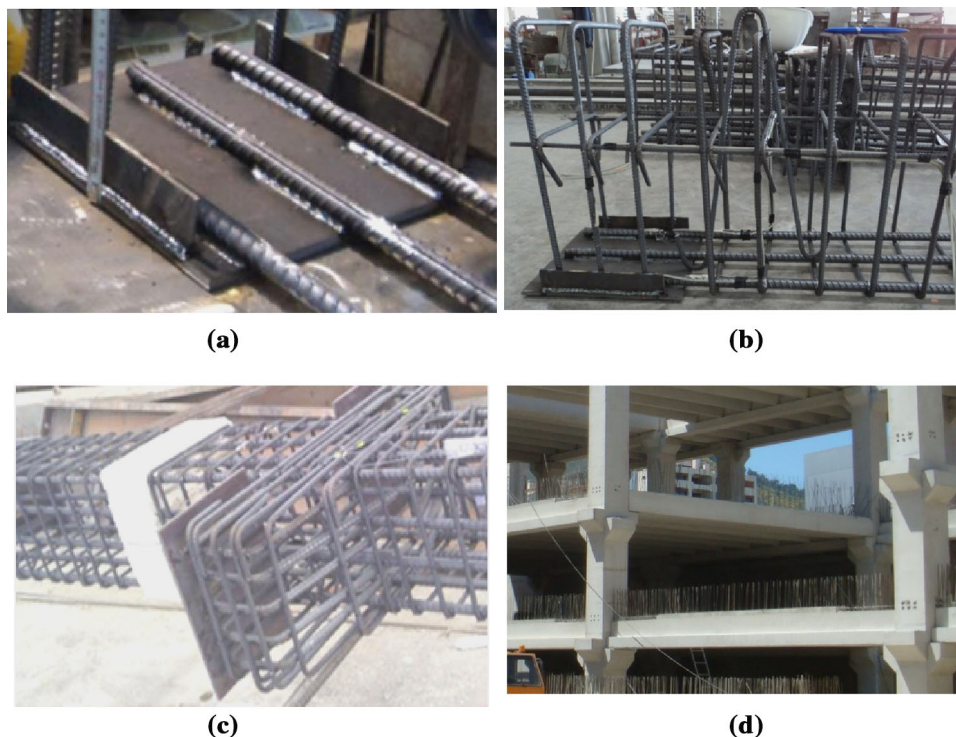


**Fig. 1** A precast structure under construction with hybrid beam-column connections. **a** Welding of longitudinal beam bottom rebars to beam end plate. **b** Installation of flexural and shear reinforcement for a precast beam. **c** Installation of flexural and shear reinforcements to constitute the precast column and corbels. **d** Assembling precast beam and column elements on site.

in precast industry. As shown in the latter sections in this study that, rebars with low carbon content (e.g. B420C grade steel) defined in TS708 code (2010) could show a sufficient ductile behavior under tensile forces after a welding process.

An experimental research program was carried out to improve the cyclic behavior of hybrid (emulative-welded) beam-column connections. In this study, half scale one monolithic and five precast specimens representing interior beam-column connections were tested under reversed cyclic loading. Strength, stiffness and energy dissipation capacities of test specimens were investigated with respect to *welding coefficient* and *unbonded length* as the main test variables. Moreover, damage indices were also obtained to compare the seismic performance of these test specimens.

## 2. Experimental Study

### 2.1 Material Tests

Weldability and hence the mechanical properties of a reinforcement after welding depend on the chemical composition of the material defined as carbon content (C) and carbon equivalent (CE) ratios (Atakoy 2014; TS 708 2010; ASTM A706M 2013). Therefore, appropriate type of longitudinal rebars which is compatible with the upper limits specified by the TS 708 code (2010) (C: 0.22%, CE: 0.50%) were installed to beam and column sections except one specimen. The rebars were also satisfying the carbon content and CE allowable limits (C: 0.30%, CE: 0.55%) given in ASTM A706M (2013) for Grade 60 rebars which has similar mechanical characteristics.

In order to characterize the tensile behavior of the rebars welded to steel plate representing the rebar-plate connection subassembly in the test specimens, tensile test was performed on 18 mm diameter reinforcing bars welded from

both sides to PL plate (St 37 steel) as shown in Fig. 2a. Appropriate electrodes (E42 type) were used to weld rebars to plate providing filler metal requirements due to TS EN ISO 2560 (2013). Figure 2b shows the specimen during testing while average strains in rebar were determined by using optical sensors focused on two points located at the vicinity of the plate.

Rebar rupture occurred within the unwelded part of the rebar specimen at 9.5% strain with a clear necked region verifying a ductile behavior under tension as shown in Fig. 2c. A tensile test was also performed on single rebar (not welded to plate) where tensile strain at rupture is determined as 12%. While interpreting the decrease in tension strain in the case of welded rebar, potential stress concentrations near the plate and heat-affected zones should be kept in mind. Besides, it is concluded that using proper type of reinforcement didn't lead to a brittle failure. The stress-strain curves gathered from the tensile tests for single and welded rebars are shown in Fig. 3.

Tensile test results of longitudinal and transverse rebars are given in Table 1. Average cylindrical concrete compressive strength ( $f_{cm}$ ) for the monolithic specimen, for beam and column precast elements, and the topping concrete were 37, 42, and 35 MPa at the test days.

### 2.2 Test Specimens

Half scale test specimens were designed in accordance with Turkish Earthquake Code (TEC 2007) and ACI 352R (2002) requirements representing an interior connection between inflection points of beam and column elements of a four-story precast building with moment frames of high ductility level. For interior beam-column joints, bond requirements are specified by ACI 318 (2011) (Eq. 1) and ACI 352R (2002) (Eq. 2) for column depth-to-beam rebar diameter ratio ( $h_c/d_b$ ) which are given in the following equations.

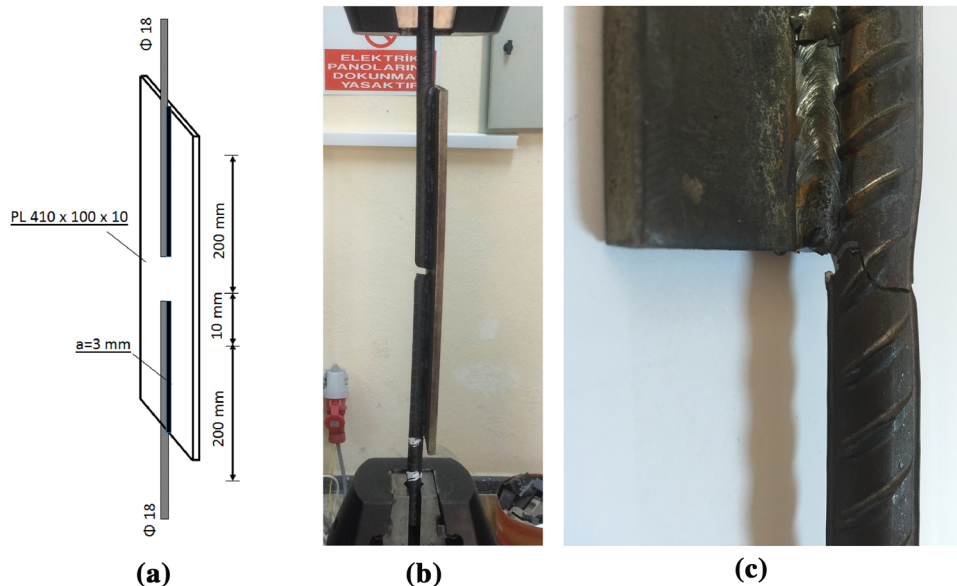


**Fig. 2** a Schematic view of welded rebar-plate specimen, b specimen during tensile test, and c rupture of rebar with a clear necked region.

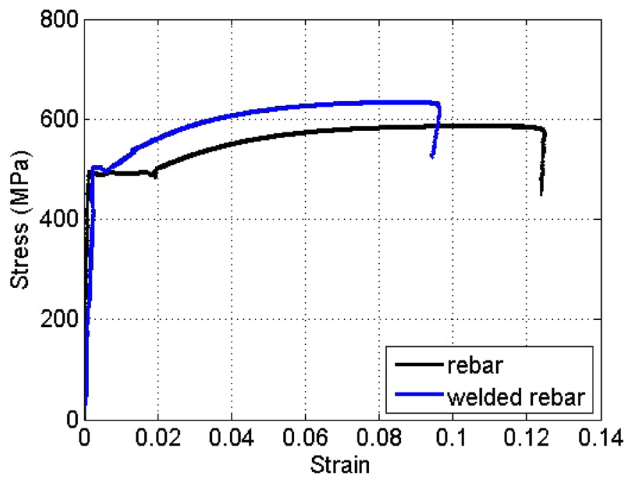


**Fig. 3** Tensile test results for an 18 mm diameter single rebar and a rebar welded to plate.

$$\frac{h_c}{d_b} \geq 20 \quad (1)$$

$$\frac{h_c}{d_b} \geq 20 \frac{f_y}{420} \geq 20 \quad (2)$$

For  $h_c$  (= 400 mm),  $d_b$  (= 18 mm) and  $f_y$  (= 461 MPa) monolithic beam-column joint fulfils the bond requirements in Eqs. (1) and (2).

Applied axial load was 8% of axial load capacity of the column during cyclic reversals. In order to investigate the failure modes in the vicinity of the connections, columns were designed to have a restricted damage during testing. Ultimate moment ratio of column-to-beam was 2.4. Longitudinal rebars were 22 mm in diameter for columns and 18 mm for beams, while 10 mm rebars were used for transverse reinforcement. Geometry and reinforcing details of the monolithic specimen are shown in Fig. 4.

Geometry, reinforcing and welding details of the precast connections are also shown in Fig. 5. During the first stage of the study, SP1, SP2, and SP3 specimens with various *welding coefficients* ( $\alpha$ ) were tested. For welded connections of precast concrete structures, seismic connection forces are multiplied by a *welding coefficient* ( $\alpha$ ) to obtain the design forces in the scope of Turkish Earthquake Code (2007). Welding coefficient was recommended as 2 and 1.5 in TEC (1998) and TEC (2007) codes, respectively. Therefore, the required area for welding between beam bottom longitudinal rebars and beam support plate (PL-1) shown in Fig. 6a was calculated by  $\alpha \times F_y$  where  $F_y$  is the yield force of a beam bottom longitudinal rebar. Corbel lengths ( $L_c$ ) of specimens

were determined considering the welding length ( $L_w$ ) of beam longitudinal rebars as given in Table 2. Minimum welding thickness ( $a_{min}$ ) was considered as 3 mm. Two additional vertical plates ( $2 \times$  PL-2) were welded to beam end plate (PL-1) to provide an extra welding area for stirrups in order to improve the connection between the stirrups and the end plate as shown in Fig. 6b.

Before the construction process of the test specimens at the laboratory shown in Fig. 7, beam and column elements of precast specimens were constructed separately in a precast facility and then transported to the laboratory. Columns were kept in a vertical position and Beam 1 and Beam 2 elements were supported on the corbel plates (PL-3). Beam end plates (PL-1) were welded to corbel plate (PL-3) at both sides with a 7 mm thick welding. 20 mm gaps were deliberately left between beam and column vertical faces at each side of the column and filled with grout properly (Fig. 7a). Beam top longitudinal rebars were placed and a topping concrete with a thickness of 150 mm was casted for the completion of specimens (Fig. 7b).

Geometry and reinforcing details of the precast specimens are given in Fig. 8. Free ends of the beams were fixed in vertical direction, 1800 mm far from the column axis while column was supported with a hinge at the bottom. Shear span to beam depth ( $a/d$ ) ratio for the specimens are about 3.

At the second stage, SP1 and SP3 specimens were improved considering the failure modes observed in the previous tests. SP1-R and SP3-R represents the revised specimens by adapting the unbonded length concept, generally applied in post-tensioned connections. Unbonded lengths ( $L_u$ ) for precast connections are proposed between 100 and 200 mm or  $4d_b - 8d_b$ , where  $d_b$  is longitudinal rebar diameter by ACI 550.2R (2013) as a design guide for precast jointed systems. Unbonded lengths in the revised specimens were considered as  $5d_b$  and  $10d_b$  for SP1-R and SP3-R specimens, respectively. Turkish Earthquake Code (2007) specifies transverse reinforcement spacing as a minimum of  $8d_b$ , 150 mm and  $0.25h_b$ , where  $h_b$  is the beam depth. For SP3-R specimen, stirrup spacing ( $s_h$ ) of beams was decreased to 75 mm and additional ties were installed to reduce possible buckling of rebars. Application of unbonded length and reinforcing details of SP3-R specimen which has a decreased welding coefficient but an increased ratio of additional ties compare to SP1-R is shown in Fig. 9.

Table 2 summarizes the welding coefficient ( $\alpha$ ), corbel length ( $L_c$ ), transverse reinforcement ratio ( $\rho_w$ ), slenderness ratio of longitudinal rebars ( $s_h/d_b$ ), applied unbonded length ( $L_u$ ), the carbon content (C) and the CE ratio of the longitudinal bars corresponding to each precast specimen.

**Table 1** Tensile test results for longitudinal and transverse rebars.

Rebar	$f_y$ (MPa)	$\epsilon_y$	$f_u$ (MPa)	$\epsilon_u$
$\phi 10$	485	0.0025	589	0.12
$\phi 18$	461	0.0024	596	0.12
$\phi 22$	490	0.0024	600	0.11

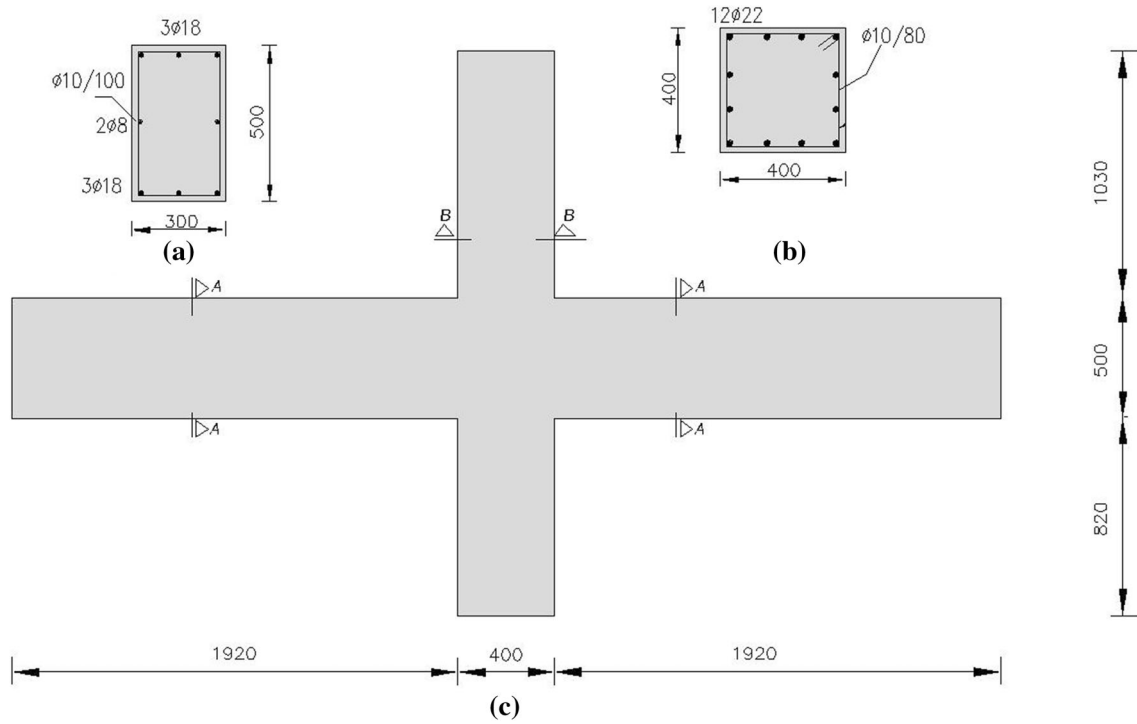


**Fig. 4** Geometry and reinforcing details for monolithic specimen **a** beam section, **b** column section, and **c** interior connection.

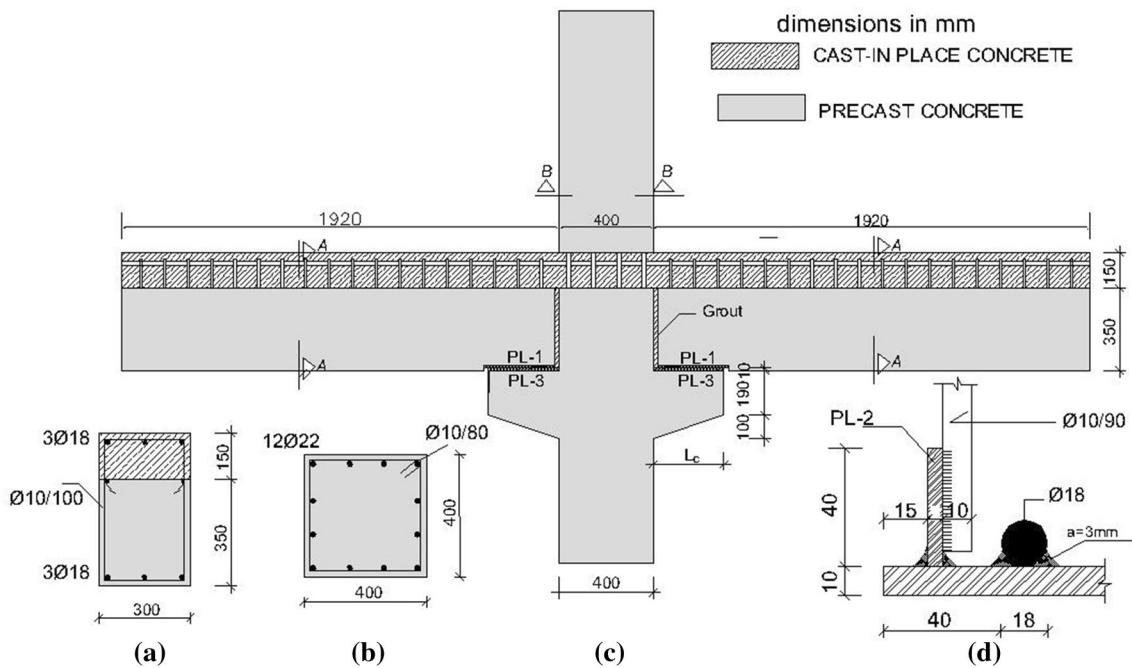


**Fig. 5** **a** Beam, **b** column cross-sections, **c** front view and dimensions of the hybrid beam-column connections, and **d** welding detail of beam bottom longitudinal rebars to beam support plate (PL-1) and stirrups to vertical plates (PL-2) for SP1, SP2 and SP3 specimens.

### 2.3 Experimental Set-up

Location of a specimen in the test set-up is shown in Fig. 10. Experimental set-up was designed and the tests were performed based on the criteria stipulated by ACI 374.1 (2005). Drift ratios are defined considering the uncertainties in strong ground motions and structural properties for beam-column connection sub-systems. Therefore, tests were continued up to 3.5% drift ratio to observe the full

post-yield behavior of the connections required by ACI 374.1 (2005).

Lateral cyclic displacement protocol adopted based on ACI 374.1 (2005) were applied to top of the column with an increasing amplitude from 0.15 to 5.0% drift ratios. Drift ratio is defined as  $\Delta/H_c$ , where  $\Delta$  is lateral displacement and  $H_c$  is the height of the column between hinges. Predefined loading protocol is shown in Fig. 11.

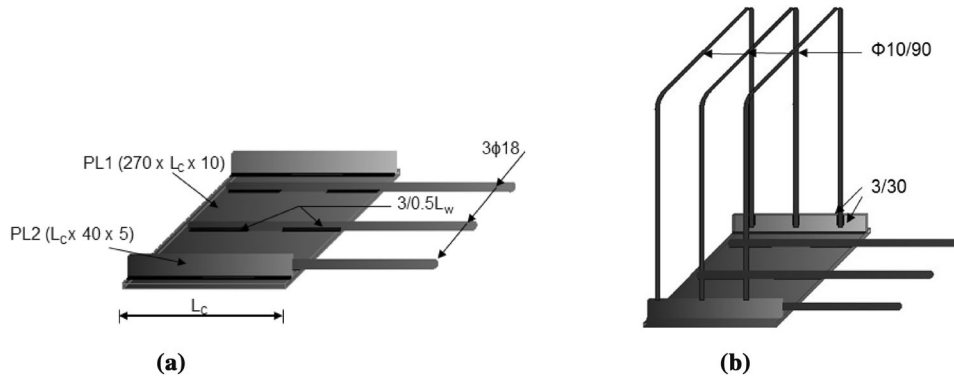


**Fig. 6** a Perspective view of beam longitudinal rebars welded to beam support plate (PL-1) and b stirrups welded to additional vertical plates ( $2 \times$  PL-2).

**Table 2** Main test parameters and properties of precast concrete interior connections.

Specimen	$\alpha$	$L_c$ (mm)	$L_w$ (mm)	$\rho_w$ (%)	$s_h/d_b$	$L_u$ (mm)	C (%)	CE (%)
SP1	2.0	450	340	0.52	5.6	N.A.	0.31	0.49
SP2	1.5	350	250	0.52	5.6	N.A.	0.19	0.35
SP3	1.2	300	200	0.52	5.6	N.A.	0.196	0.37
SP1-R	2.0	450	340	0.52	5.6	$5 d_b$	0.19	0.35
SP3-R	1.2	300	200	1.0	4.2	$10 d_b$	0.196	0.34

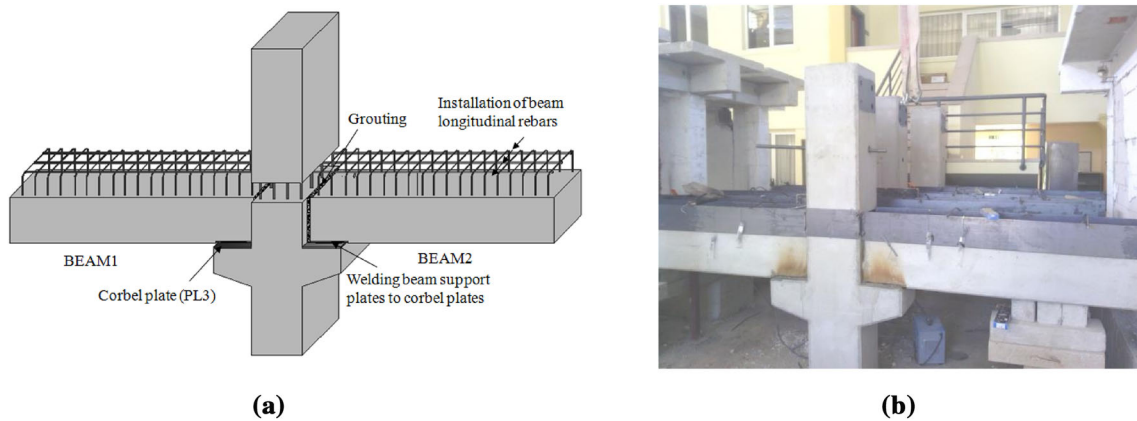


**Fig. 7** a Installation process of precast beam-column connection specimens and b casting of topping concrete.

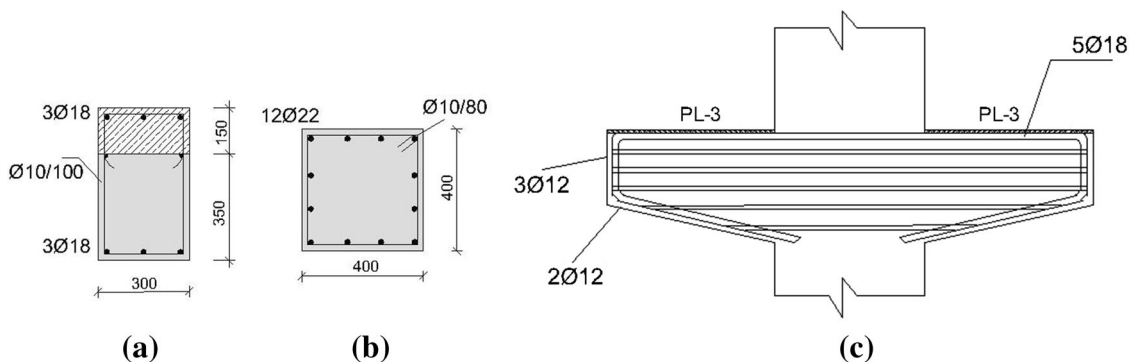


**Fig. 8** Geometry and reinforcing details of precast specimens, a beam cross section, b column cross section, and c corbel details.

In order to monitor deformations, 12 linear variable displacement transducers (LVDT) were installed by 300 mm spacing in vertical and horizontal directions. Installation of

LVDT's are shown in Fig. 12a for MONO, SP1-R, SP3; and in Fig. 12b for SP1, SP2, SP3-R specimens. Also, two string pots were installed at the top of the column to monitor the

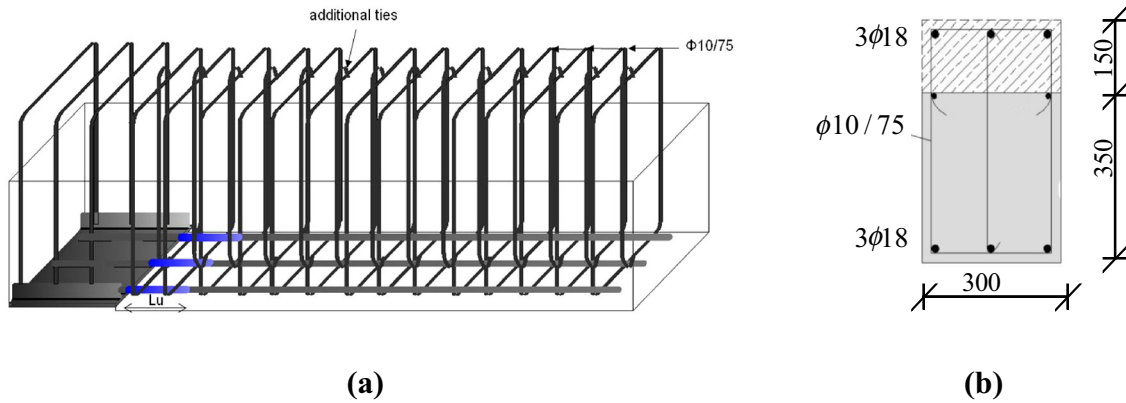


Fig. 9 a Application of unbonded length and b beam cross-section details of SP3-R specimen.

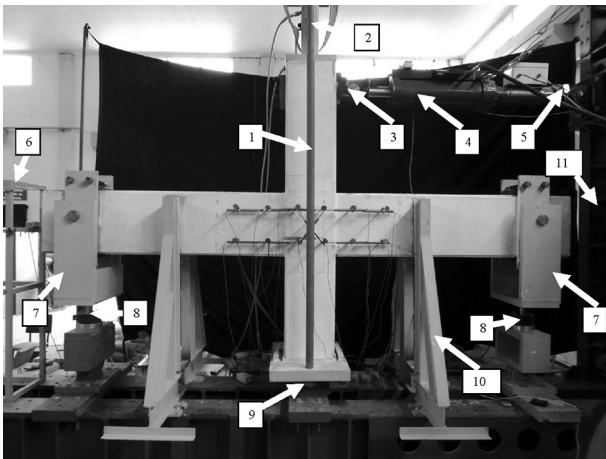


Fig. 10 Components in experimental set-up: (1) axial load frame, (2) hydraulic jack, (3) hinge, (4) actuator, (5) load cell, (6) reference frame, (7) pendulum support, (8) load cell, (9) fixed support, (10) out-of-plane support frame, (11) steel reaction frame.

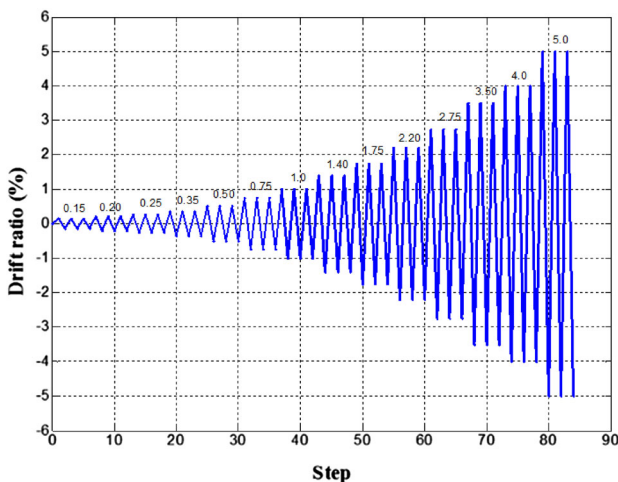


Fig. 11 Loading protocol.

applied top displacements. Strain gauges were mounted on beam and column longitudinal and transverse rebars to monitor strains throughout the tests as shown in Fig. 13.

### 3. Experimental Results

#### 3.1 Damage Patterns

Tests were continued up to certain drift ratios where the connection specimens showed significant strength degradation during loading. Figure 14 shows the damage patterns at each drift ratio for monolithic and precast connection specimens. In Fig. 14, concrete crushing is represented by shaded areas. Flexure, shear and bond failures were concentrated near the joint of the MONO specimen as shown in Fig. 14a. In the MONO specimen, bond slip of beam longitudinal rebars occurred after 2.75% drift ratio.

For precast connection specimens, flexure and shear cracks occurred along the beams while columns had only hairline joint cracks. During the experimental studies, rebar buckling and the subsequent rupture of welded beam longitudinal rebars were observed by mainly a visual inspection with the spalling of cover concrete. Damaged specimen photos showing the initiation of rebar buckling and the rupture of rebars for SP1 specimen is given in Fig. 15. Drift ratios corresponding to initiation of each damage state observed on the specimens throughout the experimental study are given in Table 3.

Beam longitudinal rebars of precast specimens welded to end plates buckled and sequentially or subsequently ruptured in most cases except for improved SP3-R specimen. Since SP1 specimen had welded rebars with CE similar to ASTM A615 type rebars (ASTM 1992) as shown in Table 2, rebar rupture occurred at a relatively lower drift ratio (2.2%) compared to revised precast specimen (SP1-R). SP2 and SP3 specimens had lower carbon content and concrete crushing at 2.75% drift (Fig. 14d) followed by rebar buckling and rupture were observed in these specimens. In SP1-R specimen, provided additional ties improved the behavior and prevented early rebar buckling. Moreover, the combination of applying unbonded length and additional vertical ties could postpone the rebar buckling in SP1-R and SP3-R specimens, and subsequently the rebar rupture.

#### 3.2 Lateral Load–Drift Ratio Relationships

Lateral load–drift ratio relationships for monolithic and precast connection specimens are shown in Fig. 16. MONO



Fig. 12 Installation of LVDTs for a MONO, SP1-R, SP3 and b SP1, SP2, and SP3-R specimens.

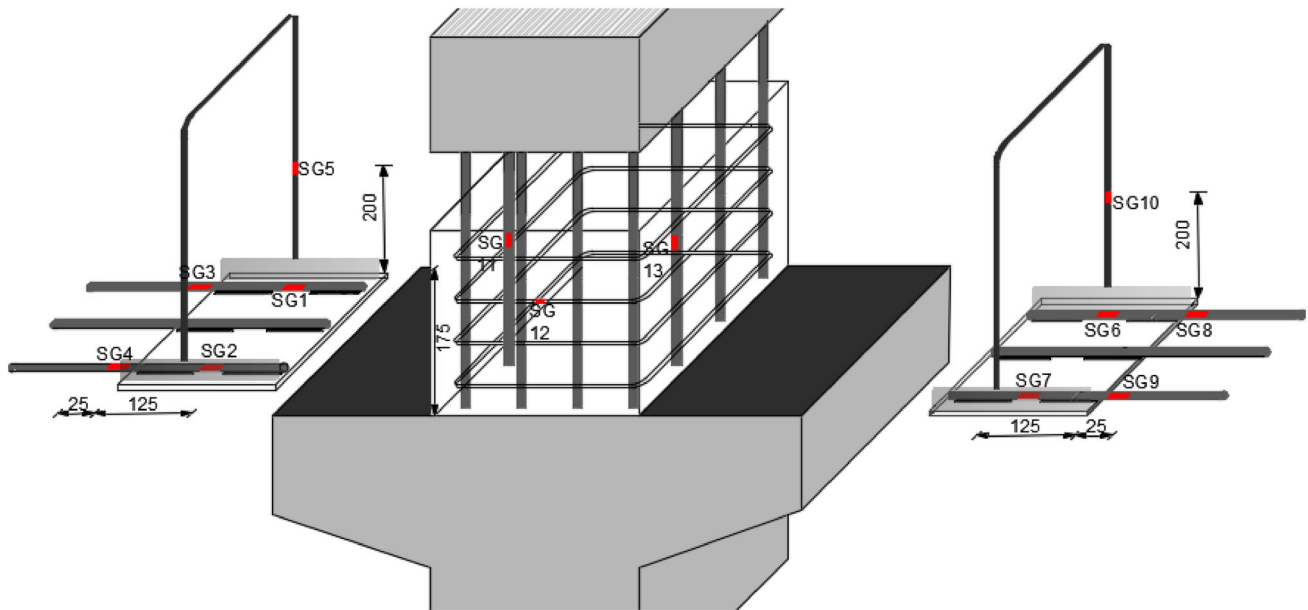


Fig. 13 Installation of strain gauges on beams and column reinforcing bars (units in mm).

specimen attained the maximum strength at 1.75% drift ratio. Severe pinching in load–drift relation was observed due to bond slip of beam longitudinal rebars at 2.75% drift ratio as seen in Fig. 16a where bond requirements were satisfied given by the codes (ACI 352 2002; ACI 318 2011). As the embedment length (equals to column depth) of beam reinforcing bars within the beam–column joint decreases, rebar slip will increase and result in a more pinched hysteretic plot (Moehle 2014). For precast connections, beam bottom longitudinal rebars were welded and only top rebars have continuity throughout the joint. Embedment lengths of top rebars could be increased from column depth ( $h_c$ ) to a length with the sum of column depth and corbel lengths ( $h_c + L_c$ ) which led to an increased energy dissipation capacity.

In SP1 specimen, maximum strength was attained at 2.2% drift ratio in the pull and push directions as shown in Fig. 16b. 40% degradation in strength for SP1 specimen was observed due to premature failure of beam welded longitudinal rebars. SP2 and SP3 specimens showed similar

behavior and maximum strengths were attained at 2.2% drift ratio as shown in Fig. 16c, d.

In SP1-R specimen, tests were performed up to 5% and 3.5% drift ratios in push and pull directions as shown in Fig. 16e, respectively. SP1-R specimen showed a more ductile behavior compare to SP1 specimen. However, shear failures after 3.5% drift ratio led severe pinching as can be seen in load–drift relationship. SP3-R specimen attained maximum strength at 2.2% drift ratio and first degradation in strength was observed at the second cycle of 3.5 drift ratio as shown in Fig. 16f.

### 3.3 Local Response

Beam curvatures, strain in reinforcing bars and shear deformations were determined for each specimen based on experimental measurements to obtain local response quantities. Beam curvatures in connection specimens were calculated based on the data taken from LVDTs (1 and 2) mounted on the connection region which includes beam ends and the joint panel as shown in Fig. 12b. For all specimens,

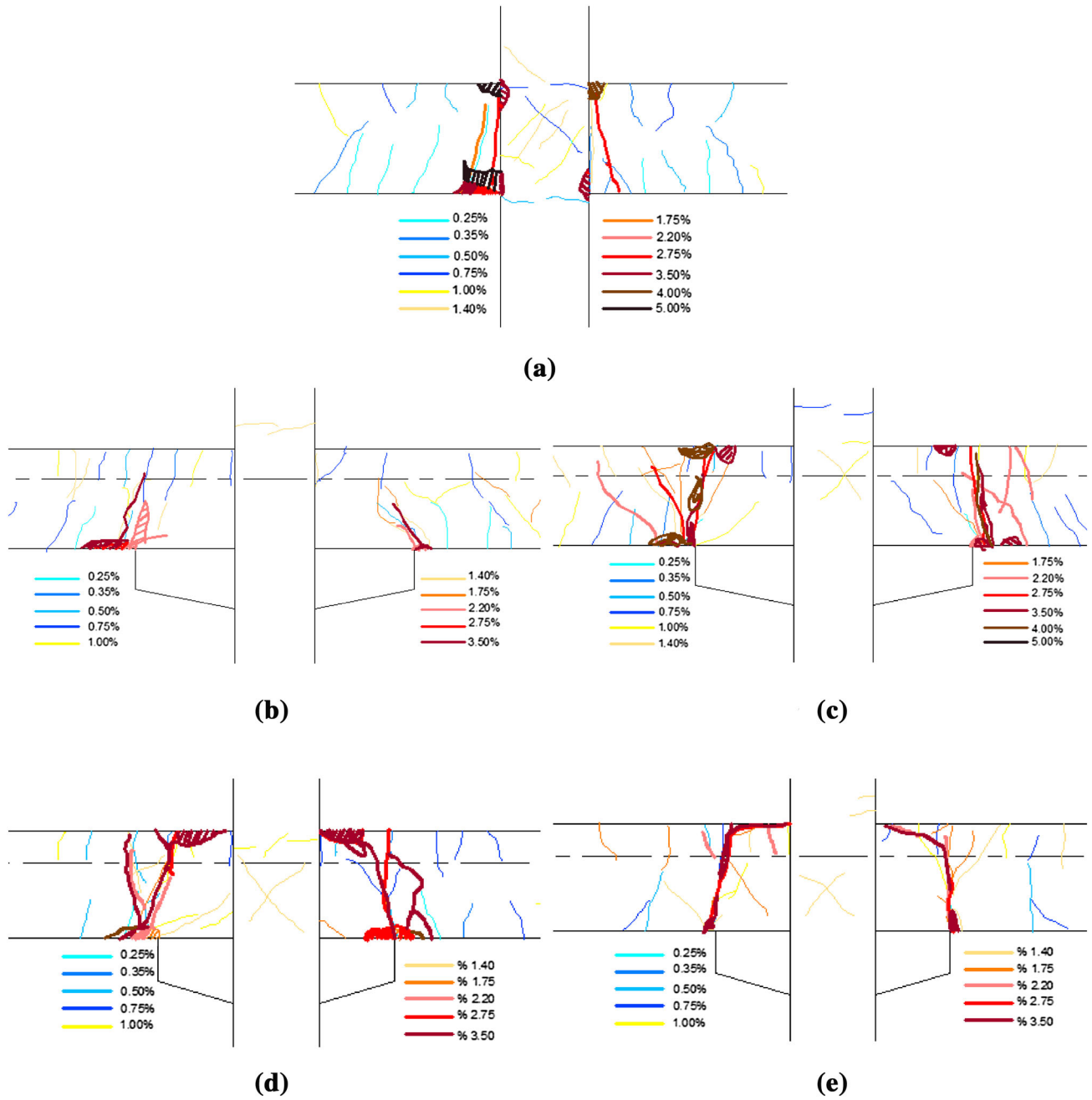


**Fig. 14** Damage patterns of test specimens at each drift ratio and the end of test. **a** MONO, **b** SP1, **c** SP1-R, **d** SP3, and **e** SP3-R.



**Fig. 15** **a** Initiation of rebar buckling at the left beam (Beam 1) and **b** the rupture of rebars at the right beam (Beam 2) for SP1 specimen at 2.2% top drift.

**Table 3** Drift ratios corresponding to initiation of each observed damage state.

Specimen	Flexural crack (%)	Shear crack (%)	Diagonal cracks in joint panel (%)	Concrete spalling (%)	Rebar buckling	Rebar rupture
MONO	0.25	1.0	1.4	2.75	N.A.	N.A.
SP1	0.25	0.5	1.75	2.2	2.2% (2nd cycle)	2.2% (2nd cycle)
SP2	0.35	0.75	1.4	2.2	2.75%	3.5% (2nd cycle)
SP3	0.25	0.75	1.4	2.2	2.75%	3.5% (1st cycle)
SP1-R	0.25	0.75	1.4	2.75	3.5% (1st cycle)	3.5% (3rd cycle)
SP3-R	0.35	1.0	1.4	2.75	N.A.	3.5% (3rd cycle)

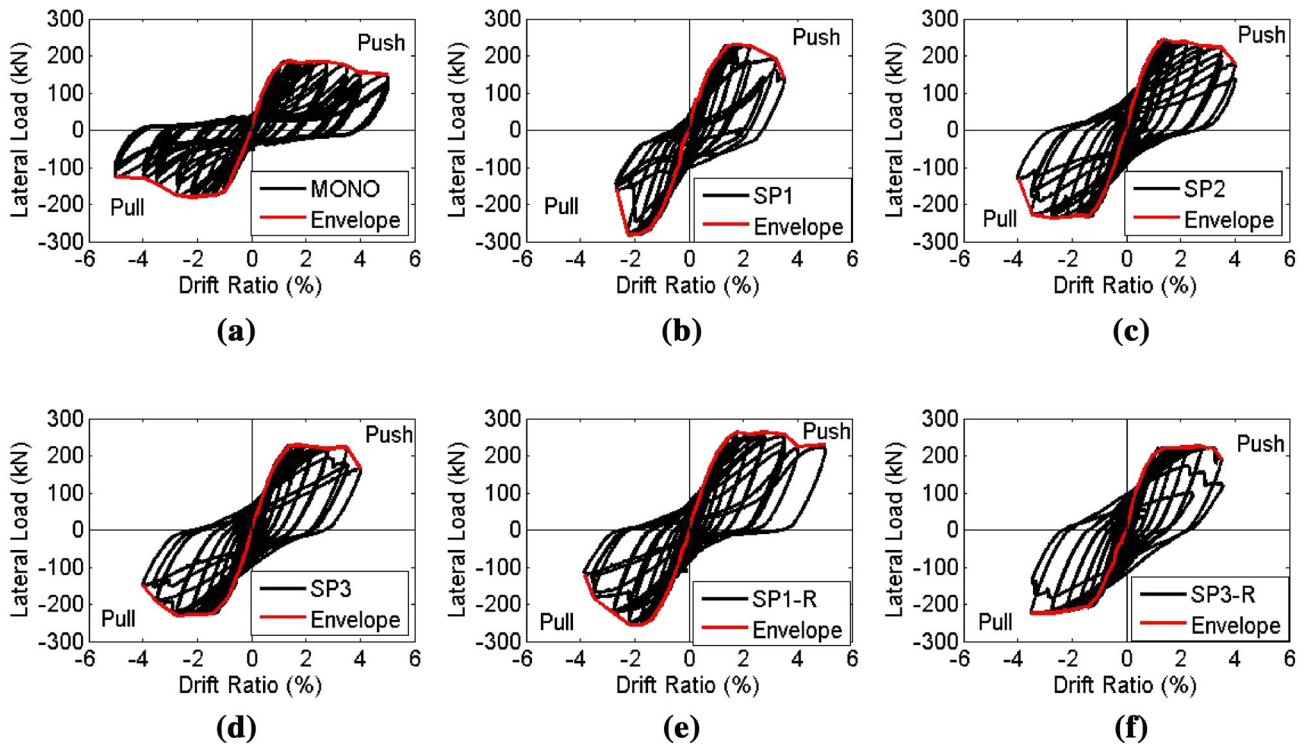


**Fig. 16** Lateral load–drift ratio relationships for monolithic and precast connection specimens.

moments were determined for Beam 1 element (Fig. 7a) at the joint face using the data taken from load cell which is embedded in the pendulum support. Figure 17 shows moment–curvature relationships for beams of beam–column connection specimens.

Measured strains of beam and column longitudinal rebars of all specimens are shown in Fig. 18 where strain gauge locations are given in Fig. 13. Large plastic strains in the beam longitudinal rebars were developed in the vicinity of the welded connections as shown in Fig. 18a–e. Drift ratios at which the strain gauge capacities exceeded the strain limit of the gauges are also noted in the figures. In SP1-R and SP3-R specimens, application of unbonded length could be able to increase the number of strain cycles of welded longitudinal rebars as well as plastic deformation capacities. On the other hand, column longitudinal rebars remained nearly elastic during the tests as shown in Fig. 18f–i.

Shear deformations of beams ( $\Delta_s$ ) in the vicinity of connections of SP1, SP2 and SP3-R specimens were calculated

based on the measurements using D1 and D2 transducers shown in Fig. 12b. Shear deformations are calculated as,

$$\Delta_s = \frac{(D2 - D1)}{2 \sin \theta} \quad (3)$$

where  $\theta$  is the inclination angle of diagonal LVDT's ( $45^\circ$ ) with respect to horizontal axis with Fig. 19 shows beam shear force–shear deformation relationships. In SP3-R specimen which has additional vertical ties and more frequent transverse reinforcement, shear deformations in beam elements could be reduced reasonably.

## 4. Evaluation of Experimental Results

### 4.1 Lateral Strength and Ductility

Lateral load–drift ratio envelopes of test specimens were obtained by combining the maximum lateral loads corresponding to each drift ratio. *Component Equivalency*

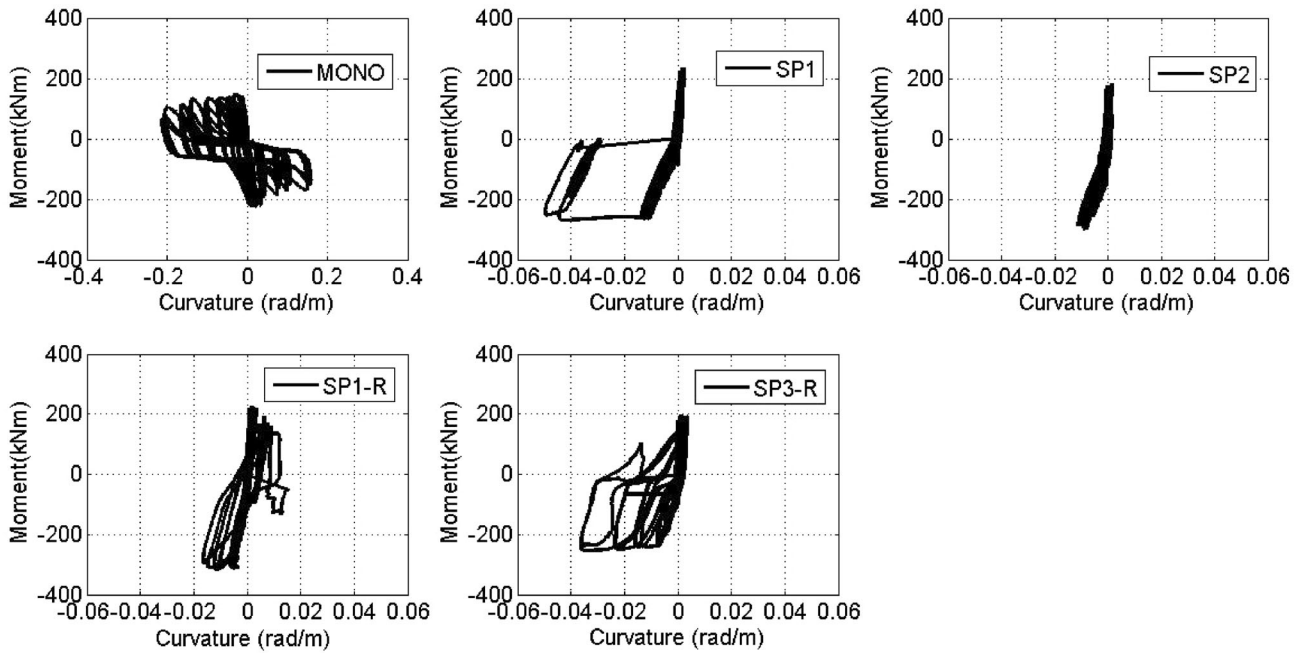


Fig. 17 Moment-curvature relationships of beam-column connection specimens.

Methodology defined in FEMA P-795 (2011) quantifies the strength, ductility and initial stiffnesses as shown in Fig. 20. Ultimate drift ratio ( $\theta_U$ ) corresponds to 80% of the ultimate strength ( $Q_M$ ). Also, effective yield drift ratio ( $\theta_{Y,eff}$ ) and initial stiffness ( $K_i$ ) can be obtained by intersecting the lines crossing the  $0.4Q_M$  and  $Q_M$  as shown in Fig. 20.

Figure 21a shows the lateral load–drift ratio envelopes of test specimens, and normalized strength with respect to yield strength ( $Q/Q_y$ ) are shown in Fig. 21b. Ultimate strength, drift ratio and effective ductility of test specimens are summarized in Table 4. Although the tests were continued up to higher drift ratios to investigate further failure modes, ultimate drift ratios ( $\theta_U$  [%]) do not correspond to these drifts where the tests finalized. Ultimate drift ratios corresponding to 80% of the ultimate strengths ( $Q_M$ ) are determined for both push and pull directions, and the minimum of these drift ratios are taken into account for ductilities of each test specimen. In this regard, changing the details for welding of rebars showed a significant effect on improving the seismic response. SP1 specimen beams reinforced with relatively high carbon content bars showed an abrupt decrease in strength at 2.2% drift ratio. However, SP2 and SP3 specimens showed a gradual strength degradation up to 3.5 drift ratio.

Acceptance criteria for moment frames based on structural testing (ACI 374.1 2005) requires that strength of specimens at the third cycle of 3.5% drift ratio ( $Q_{3.5}$ ) should not be less than  $0.75Q_M$ . Since in-cycle strength degradation was caused by abrupt rupture of welded reinforcing bars for precast specimens, this condition was provided by SP1-R and SP3-R specimens only as indicated in Table 4— $Q_{3.5}$  column.

Displacement ductility ( $\mu_e$ ) of a connection specimen is the ratio of ultimate drift ratio ( $\theta_U$ ) to the effective yield drift ratio ( $\theta_e$ ). Displacement ductility of each specimen is

shown in Table 4. SP3-R had higher displacement ductility among the precast specimens after the achieved improvements.

#### 4.2 Lateral Stiffness

Secant stiffness ( $K_{sec}$ ) can be calculated as the slope of the line between the lateral load and corresponding drift ratios as shown in Fig. 22. ACI 374.1 (2005) requires that secant stiffness calculated at the third cycle of 3.5% drift ratio ( $K_{3.5}$ ) should not be less than 0.05 of the initial stiffness ( $K_i$ ). Initial stiffnesses of test specimens are given in Table 5 and secant stiffnesses at 3.5% drift ratio were provided by all specimens except for SP1 specimen.

Secant stiffnesses of test specimens were normalized based on the stiffness at first cycle of 0.15% drift ratio and shown in Fig. 23. MONO specimen showed faster stiffness degradation than the precast specimens up to 2% drift ratio. SP1 and SP1-R specimens showed 58% degradation up to 2.2% drift ratio, however SP1 showed a sudden decrease in stiffness at 2.2% drift ratio. Besides, SP2, SP3 and SP3-R specimens showed a gradual decrease in stiffness during the experiments.

#### 4.3 Energy Dissipation

Energy dissipation of monolithic and precast specimens are compared by using relative energy dissipation ratios ( $\beta_i$ ). Relative energy dissipation calculated at the third cycle of 3.5% drift ratio should not be less than 12.5% based on ACI 374.1 (2005) criteria. Relative energy dissipation is the ratio of energy dissipation at each drift to the ideal energy dissipation represented by the area of the parallelogram shown in Fig. 22. Relative energy dissipation ( $\beta_i$ ) can be obtained by

$$\beta_i = \frac{A_{hi}}{(E_{1i} + E_{2i})(\theta'_{1i} + \theta'_{2i})} \quad (4)$$

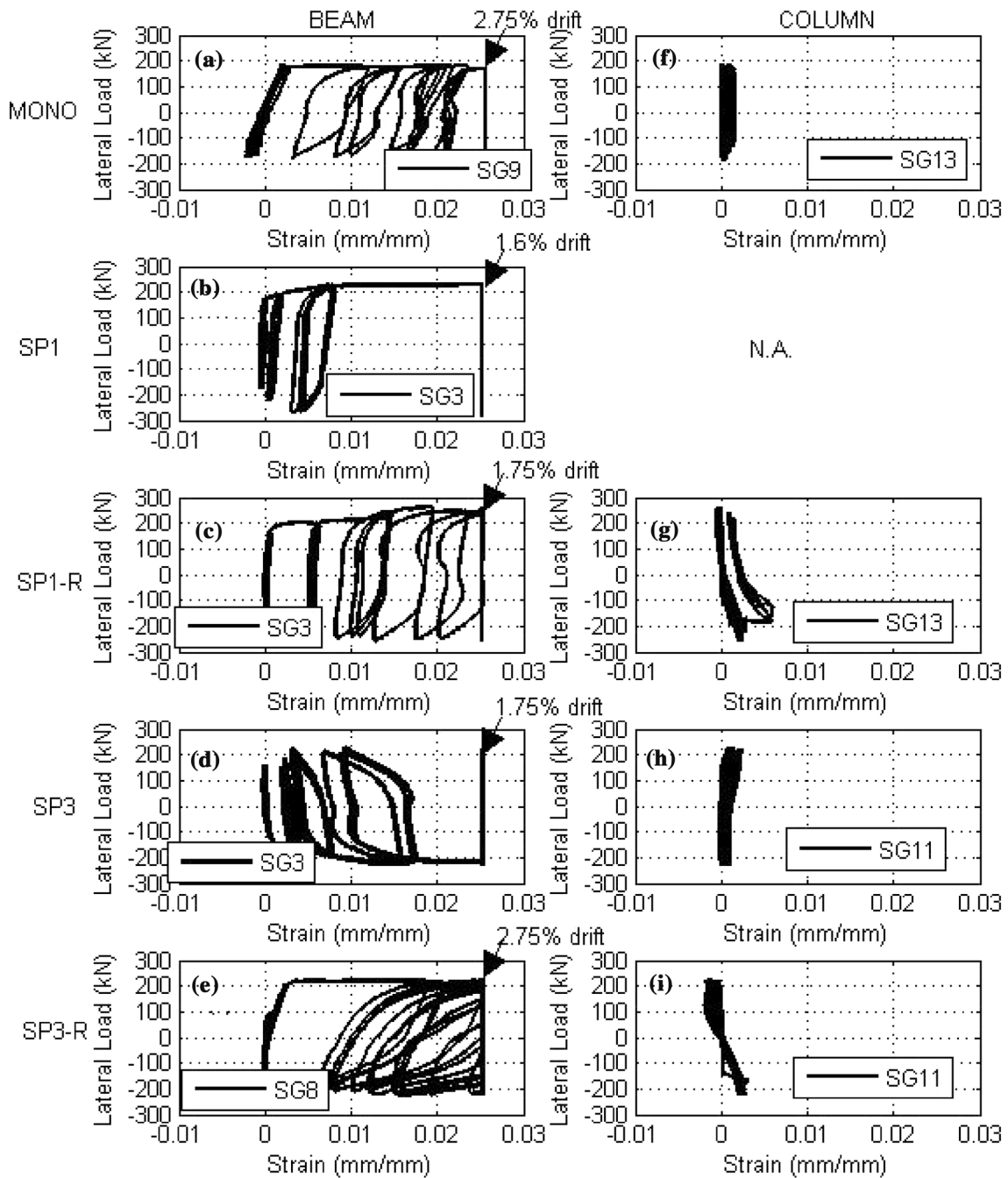


Fig. 18 Measured longitudinal bar strains of beams and columns of connection specimens.

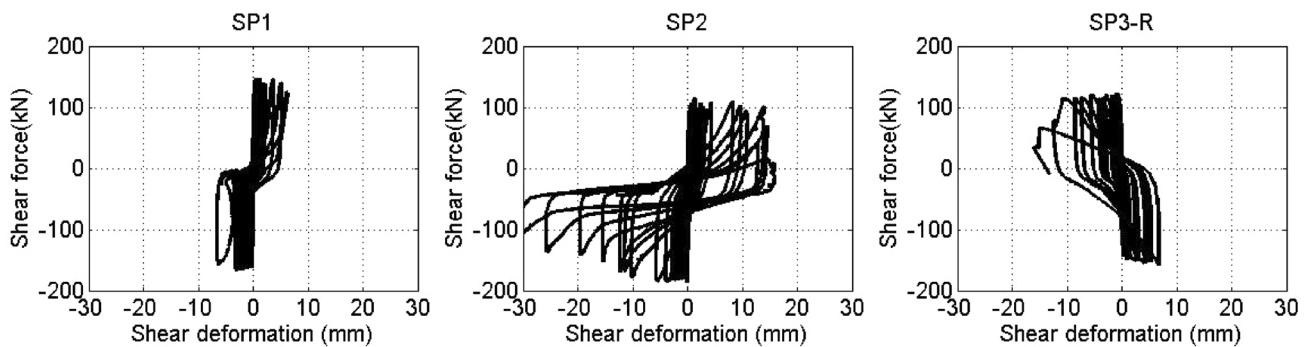


Fig. 19 Beam shear force-shear deformations relationships for SP1, SP2 and SP3-R specimens.

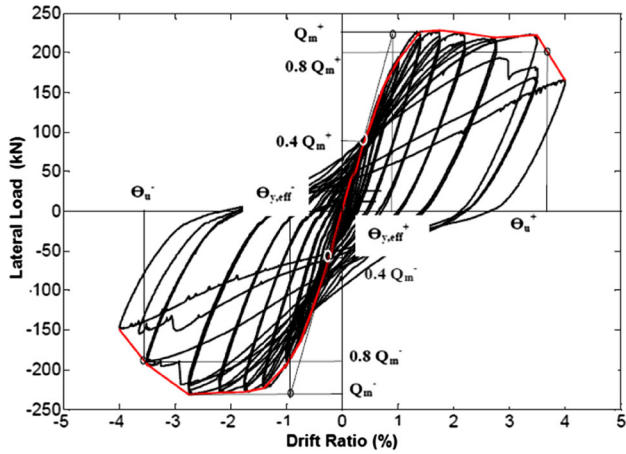


Fig. 20 Quantification of strength and ductility of test specimens.

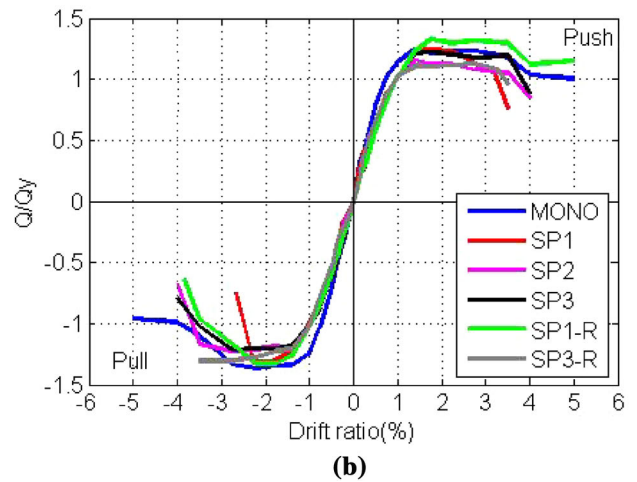
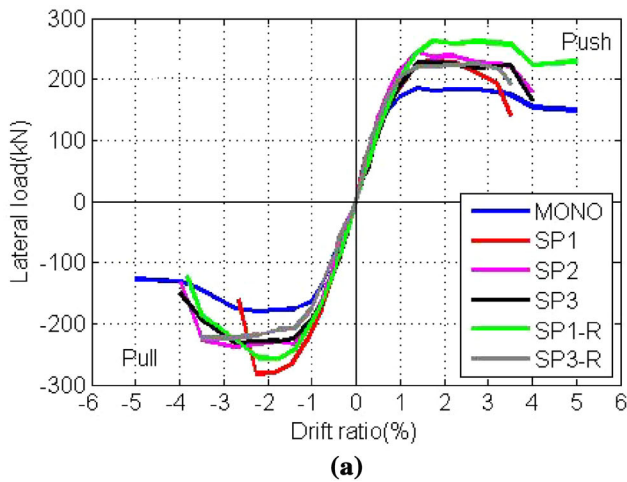


Fig. 21 a Lateral load–drift ratio envelopes of test specimens and b normalized envelopes of test specimens.

Table 4 Lateral strength and ductility of test specimens.

Specimen	Direction	$Q_M$ (kN)	$0.75 Q_M$ (kN)	$Q_{3.5}$ (kN)	$\Theta_{Y,eff}$ (%)	$\Theta_U$ (%)	$\mu_e$
MONO	Push	189.3	142.0	<b>175.5</b>	0.8	4.0	5.0
	Pull	183.8	137.9	<b>144.8</b>	0.96	3.5	3.7
SP1	Push	231.6	173.7	140.3	0.86	3.3	3.8
	Pull	287.8	215.9	N.A.	1.0	2.5	2.5
SP1-R	Push	263.2	197.4	<b>210.6</b>	1.1	5.0	4.5
	Pull	256.9	192.7	130.6	0.96	3.5	3.6
SP2	Push	249.5	187.1	179.1	0.91	3.7	4.1
	Pull	237.5	178.1	161.7	1.16	3.9	3.4
SP3	Push	231.2	173.4	168	0.9	3.9	4.3
	Pull	235.8	176.9	154.5	0.9	3.7	4.1
SP3-R	Push	225.7	169.3	125.7	0.7	3.5	5.1
	Pull	228.2	171.1	<b>173.2</b>	1.0	3.5	3.5

where  $A_{h,i}$  is the area of the closed loop of  $i$ th drift ratio,  $E_{1i}$  and  $E_{2i}$  are the strengths and  $\theta_{1i}$  and  $\theta_{2i}$  are inelastic drift ratios in both loading directions.

Figure 24 shows the relative energy dissipation relationship of test specimens corresponding to third cycle of each drift ratio.  $\beta_i$  values showed a decrease up to 1% drift ratio inherently because of the minor cracks in the test specimens. However, yielding of reinforcement and other failure mechanisms caused an increase in the ratios. All specimens fulfilled the relative energy dissipation criteria mentioned above.

#### 4.4 Damage Index

Damage index enables seismic evaluation of existing reinforced concrete buildings subjected to earthquakes. Damage indices of test specimens were calculated based on

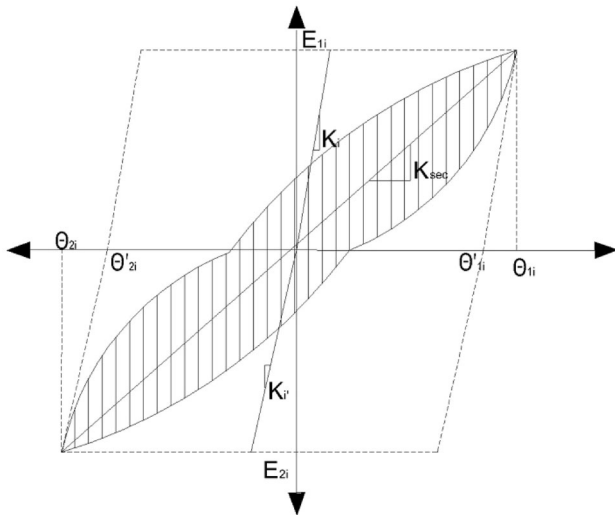


**Fig. 22** Calculation of secant stiffness ( $K_{sec}$ ) for test specimens.

strength, ductility and energy dissipation characteristics. Park and Ang (1985) stated damage index ( $D$ ) in terms of energy dissipation and displacements as

$$D = \frac{\delta_M}{\delta_U} + \beta \frac{E_H}{Q_Y \delta_U} \quad (5)$$

where  $Q_Y$  is the yield strength,  $E_H$  is the dissipated energy,  $\beta$  is strength degradation parameter  $\delta_M$  and  $\delta_U$  are maximum displacements under earthquake and monotonic loading, respectively. Ang et al. (1993) proposed the damage index at collapse state as 0.8.

Craifaleanu and Lungu (2008) derived another damage index in terms of displacement ductilities as,

$$D = \frac{\mu}{\mu_U} + \beta \frac{(\mu_E - 1)}{\mu_U} \quad (6)$$

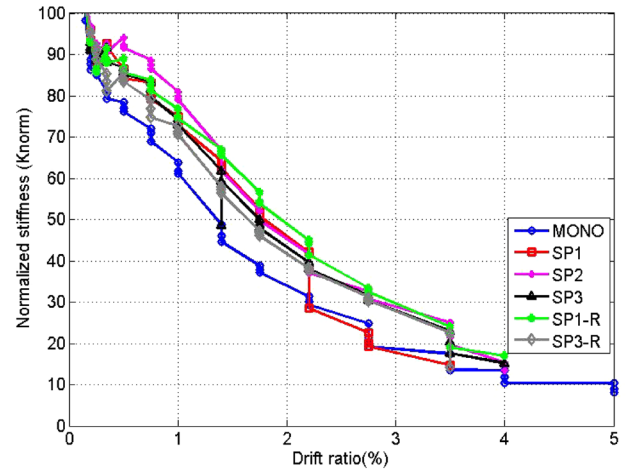


**Fig. 23** Normalized secant stiffness ( $K_{sec}$ ) of test specimens for corresponding drift ratios.

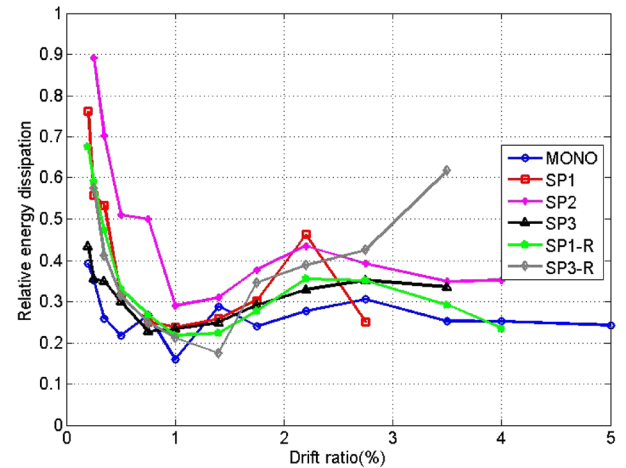


**Fig. 24** Relative energy dissipation ratios ( $\beta_i$ ) of test specimens.

**Table 5** Initial stiffnesses of test specimens.

Specimen	Direction	$K_i$ (kN/mm)	$0.05 K_i$	$K_{3.5}$ (kN/mm)
MONO	Push	10.2	0.51	0.50
	Pull	8.3	0.42	0.45
SP1	Push	11.7	0.59	N.A.
	Pull	12.5	0.63	N.A.
SP1-R	Push	10.6	0.53	1.52
	Pull	11.8	0.59	1.05
SP2	Push	11.9	0.59	1.15
	Pull	8.9	0.45	1.1
SP3	Push	11.1	0.56	1.58
	Pull	11.3	0.57	1.08
SP3-R	Push	15.7	0.79	1.93
	Pull	8.2	0.41	1.78

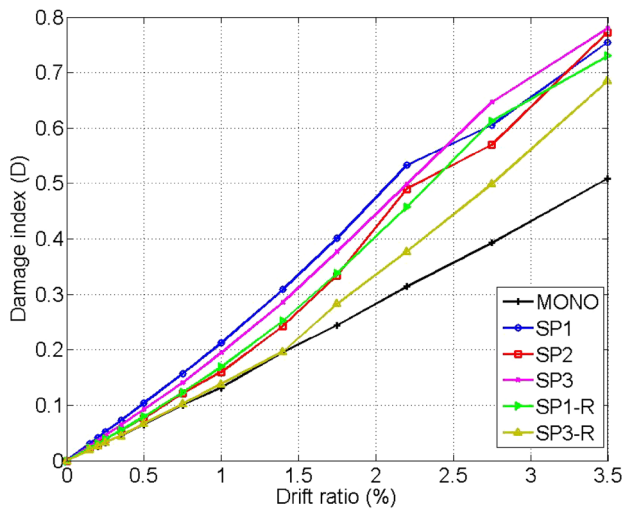


Fig. 25 Damage indices obtained for each test specimen.

Since beam-column connection tests were performed under cyclic loading, maximum displacements under monotonic loading ( $\delta_U$ ) are considered as

$$\delta_U = 2\delta_{U,cyc} \quad (7)$$

where  $\delta_{U,cyc}$  is the ultimate displacement under cyclic loading conditions based on numerical simulations.

Damage indices of test specimens for the third cycle of each drift ratio are calculated by Eq. (6) and shown in Fig. 25. Accordingly, damage index for SP1 specimen has the highest value due to observed abrupt failure while unbonded length applied in the SP1-R specimen caused lower damage index. In addition, with the improvements in the SP3-R specimen, damage index was determined to have a lower value accordingly.

## 5. Conclusions

In this study, experimental cyclic response of hybrid (emulative-welded) precast beam-column connections were investigated. Test specimens were compared in terms of strength, stiffness and energy dissipation capacities as well as damage indices.

- During the test of monolithic specimen (MONO), bond-slip of beam reinforcing bars after 3.5% drift ratio caused a pinched behavior in the force-deformation relation and decreased the energy dissipation. On the other hand, precast specimens showed increased relative energy dissipation ratios with the increase of embedment length of beam top reinforcing bars.
- Precast specimens which were tested at the first stage (without an unbonded length) didn't show similar behavior in terms of ductility as the MONO specimen showed. Strain development of beam welded rebars played an important role on the overall behavior of precast connections. SP1 specimen beams reinforced with relatively high carbon content bars showed an abrupt decrease in the strength at 2.2% drift ratio.

However, SP2 and SP3 specimens showed a gradual strength degradation up to 3.5% drift ratio. Obtained damage indices for SP1, SP2 and SP3 specimens were close to the index corresponding to collapse state contrast to MONO specimen.

- Unbonding of welded rebars within a sleeve could be able to decrease strain demands in the vicinity of the connection. SP1-R specimen showed a higher ductility than SP1 specimen but it showed severe pinching due to shear failures.
- SP3-R specimen showed an improved seismic behavior thanks to unbonded length approach and the additional ties to prevent early buckling of longitudinal bars.
- Based on the experimental findings and further evaluations, revising the relevant requirements in design codes such as maximum spacing of beam transverse reinforcement, adopting additional vertical ties and the unbonded length approach to resist early buckling and rupture of flexural rebars is proposed.

## Acknowledgements

Experimental study was supported by Turkish Precast Concrete Association and Dokuz Eylul University Scientific Research Program under the Grant No. DEU-BAP 2012.KB.FEN.019. The contributions of Dr. Sevket Ozden, M.Sc. Hakan Atakoy, M.Sc. Gunkut Barka, Dr. Turkey Baran, Dr. Ozgur Ozcelik and M.Sc. Eng. Umut Yucel to the experimental studies carried out in the Structural Mechanics Laboratory at Dokuz Eylul University are gratefully acknowledged. Tensile tests were performed in Mechanic Laboratory at Dokuz Eylul University Metallurgical and Minerals Engineering Department.

## Open Access

This article is distributed under the terms of the Creative Commons Attribution 4.0 International License (<http://creativecommons.org/licenses/by/4.0/>), which permits unrestricted use, distribution, and reproduction in any medium, provided you give appropriate credit to the original author(s) and the source, provide a link to the Creative Commons license, and indicate if changes were made.

## References

- ACI 318. (2011). *Building code requirements for structural concrete and commentary*. American Concrete Institute. Farmington Hills, MI: American Concrete Institute.
- ACI 352R. (2002). *Recommendations for design of beam-column connections in monolithic reinforced concrete structures*. Farmington Hills, MI: American Concrete Institute.
- ACI 374.1. (2005). *Acceptance criteria for moment frames based on structural testing and commentary*. Farmington Hills, MI: American Concrete Institute.

- ACI 550.2R. (2013). *Design guide for connections in precast jointed systems*. Farmington Hills, MI: American Concrete Institute.
- ACI ITG/T1.2. (2003). *Special hybrid moment frames composed of discretely jointed precast and post-tensioned concrete member and commentary*. Farmington Hills, MI: American Concrete Institute.
- Ang, A. H. S., Kim, W. J., & Kim, S. B. (1993). Damage estimation of existing bridge structures. In *Structural engineering in natural hazards mitigation: Proceedings of ASCE structures congress*, Irvine CA (Vol. 2, pp. 1137–1142).
- ASTM A615/A 615M. (1992). *Deformed and plain billet-steel bars for concrete reinforcement*. West Conshohocken, PA: ASTM International.
- ASTM A706M. (2013). *Standard specification for low-alloy steel deformed and plain bars for concrete reinforcement*. West Conshohocken, PA: ASTM International.
- Atakoy, H. (2014). Review on weldability of reinforcing steel, and design criterion for reinforced concrete applications. *Precast Concrete Journal*, 110, 5–9. **(in Turkish)**.
- Belleri, A., & Riva, P. (2012). Seismic performance and retrofit of precast concrete grouted sleeve connections. *PCI Journal*, 57(1), 97–109.
- Chang, B., Hutchinson, T., Wang, X., & Englekirk, R. (2013). Experimental seismic performance of beam-column sub-assemblies using ductile embeds. *Journal of Structural Engineering*, 139(9), 1555–1566.
- Chen, S., Yan, W., & Gao, J. (2012). Experimental investigation on the seismic performance of large-scale interior beam-column joints with composite slab. *Advances in Structural Engineering*, 15(7), 1227–1237.
- Cheok, G. S., Stone, W. C., & Lew, H. S. (1993). Performance of 1/3-scale model precast concrete beam-column connections subjected to cyclic inelastic loads. Report No. 3, NISTIR 5246, National Institute of Standard and Technology.
- Cheok, G. S., Stone, W. C., & Nakaki, S. D. (1996). Simplified design procedure for hybrid precast concrete connections. NISTIR 5765, National Institute of Standard and Technology.
- Craifaleanu, I-G., & Lungu, D. (2008). An assessment of damage potential and of building performance demands for Romanian Vrancea earthquakes. In *14th World Conference on Earthquake Engineering, Beijing, China*.
- Ertas, O., Ozden, S., & Ozturan, S. (2006). Ductile connections in precast concrete moment resisting frames. *PCI Journal*, 51(3), 66–76.
- FEMA P-795. (2011). *Quantification of building seismic performance factors: Component equivalency methodology*. Washington, DC: Federal Emergency Management Agency.
- Im, H., Park, H., & Eom, T. (2013). Cyclic loading test for reinforced-concrete emulated beam-column connection of precast concrete moment frame. *ACI Structural Journal*, 110(1), 115–125.
- Kassem, W. (2015). Strength prediction of corbels using strut-and-tie model analysis. *International Journal of Concrete Structures and Materials*, 9(2), 255–266.
- Kim, J., & Hyunhoon, C. (2015). Monotonic loading tests of RC beam-column subassembly strengthened to prevent progressive collapse. *International Journal of Concrete Structures and Materials*, 9(4), 401–413.
- Lim, K., Shin, H., Kim, D., Yoon, Y., & Lee, J. (2016). Numerical assessment of reinforcing details in beam-column joints on blast resistance. *International Journal of Concrete Structures and Materials*, 10(3), 87–96.
- Moehle, J. (2014). *Seismic design of reinforced concrete buildings*. New York: McGraw Hill Professional.
- Negro, P., & Toniolo, G. (2012). *Design guidelines for connections of precast structures under seismic actions*. Report EUR 25377 EN, European Commission.
- Ozden, S., & Meydanli, H. (2003). Seismic response of precast industrial buildings during 1999 Kocaeli earthquake. SE-40EEE, Skopje earthquake 40 years of European earthquake engineering, Skopje, Macedonia.
- Pampanin, S., Priestley, M. J., & Sriharan, S. (2001). Analytical modeling of the seismic behaviour of precast concrete frames designed with ductile connections. *Journal of Earthquake Engineering*, 5(3), 239–367.
- Park, R., & Ang, A. H. S. (1985). Mechanistic seismic damage model for reinforced concrete. *Journal of Structural Engineering*, 111(4), 722–739.
- Park, R., & Bull, D. K. (1986). Seismic resistance of frames incorporating precast prestressed concrete beam shells. *PCI Journal*, 31(4), 54–93.
- Priestley, M. J. N., Sriharan, S., Conley, J. R., & Pampanin, S. (1999). Preliminary results and conclusions from the PRESSS five-story precast concrete test building. *PCI Journal*, 44(6), 42–67.
- Rashidian, O., Abbasnia, R., Ahmadi, R., & Nav, F. M. (2016). Progressive collapse of exterior reinforced concrete beam-column sub-assemblages: Considering the effects of a transverse frame. *International Journal of Concrete Structures and Materials*, 10(4), 479–497.
- Rodriguez, M. E., & Rodriguez, A. (2006). Welding of reinforcing bars should be avoided in reinforced concrete structures in seismic zones in Mexico. *Revista de Ingenieria Sismica, Sociedad Mexicana de Ingenieria Sismica*, 75, 69–95. **(in Spanish)**.
- Rodríguez, Mario E., & Torres-Matos, Miguel. (2013). Seismic behavior of a type of welded precast concrete beam-column connection. *PCI Journal*, 58(3), 81–94.
- Ronagh, H. R., & Baji, H. (2014). On the FE modeling of FRP-retrofitted beam-column subassemblies. *International Journal of Concrete Structures and Materials*, 8(2), 141–155.
- Saatcioglu, M., Mitchell, D., Tinawi, R., Gardner, N. J., Gillies, A. G., Ghobarah, A., et al. (2001). The August 17, 1999 Kocaeli (Turkey) earthquake-damage to structures. *Canadian Journal of Civil Engineering*, 28(4), 715–737.
- Senel, S., & Palanci, M. (2013). Structural aspects and seismic performance of 1-story precast buildings in Turkey. *Journal of Performance of Constructed Facilities*, 27(4), 437–449.
- TS EN ISO 2560. (2013). Welding consumables - Covered electrodes for manual metal arc welding of non-alloy and

- fine grain steels - Classification. Ankara: Turkish Standards Institution.
- TS 708. (2010). Steel for the reinforcement of concrete—Reinforcing steel. Ankara: Turkish Standards Institution.
- Turkish Earthquake Code (TEC). (1998). *Specifications for structures built in disaster areas*. Ankara: Ministry of Public Works and Settlement.
- Turkish Earthquake Code (TEC). (2007). *Specifications for buildings constructed in disaster areas*. Ankara: Ministry of Public Works and Settlement.
- Yuksel, E., Karadogan, H. F., Bal, İ. E., Ilki, A., Bal, A., & Inci, P. (2015). Seismic behavior of two exterior beam-column connections made of normal-strength concrete developed for precast construction. *Engineering Structures*, 99, 157–172.